

# Exact and Evolutionary Algorithms for Sequential Multi-Objective Transmission Topology Planning

Job Groeneveld<sup>1</sup>, Miguel Muñoz<sup>2</sup>, Jan Viebahn\*<sup>1</sup>, and Alessandro Zocca<sup>3</sup>

<sup>1</sup>TenneT TSO B.V., Arnhem, The Netherlands

<sup>2</sup>Artelys, Paris, France

<sup>3</sup>Department of Mathematics, Vrije Universiteit Amsterdam, The Netherlands

May 6, 2026

## Abstract

We address day-ahead transmission topology planning and congestion management as a sequential, multi-objective optimization problem and develop two complementary algorithms for it: an exact enumeration method and a tailored evolutionary heuristic. The problem is formulated with four operational objectives reflecting real TSO decision criteria: worst-case line loading under  $N - 1$  security, topological depth, number of switching actions, and time spent in non-reference topologies, over a 24-hour horizon. We introduce the block algorithm, an exact method that exploits the temporal block structure of feasible strategies to enumerate the complete Pareto front; for fixed operational bounds on depth and switch count, its evaluation count grows polynomially with the planning horizon. We complement it with a multi-objective evolutionary algorithm based on NSGA-III, with structure-guided initialization and problem-specific variation operators tailored to the topology-planning structure. Using real operational data from the Dutch high-voltage grid operated by TenneT TSO, we show that the block algorithm computes the full Pareto front for a highly congested day in under three minutes, and that the evolutionary algorithm converges toward but does not recover the exact front. The block algorithm thus provides both a practical decision-support tool and a ground-truth benchmark for future heuristic and learning-based methods on this problem class.

## 1 Introduction

Electricity grids worldwide are struggling to keep pace with the rapid deployment of renewable generation and the electrification of end uses. The International Energy Agency has identified grid congestion as a growing threat to energy security and clean energy transitions, noting that over 1 500 GW of renewable projects are in advanced stages of development but awaiting grid connections [22]. In the European Union, the cost of managing grid congestion through remedial actions such as redispatching reached 4.3 billion euros in 2024, corresponding to 60 TWh of adjusted generation. In the Netherlands, where this study is situated, the transmission system operator TenneT spent 388 million euros on congestion management in 2022, more than six times the amount spent in 2020 [23]. These trends underscore the urgent need for cost-effective operational measures that can relieve congestion using existing infrastructure, without requiring new transmission lines or costly generation redispatching.

Transmission system operators (TSOs) are responsible for managing congestion of high-voltage transmission grids. This task involves performing network security analyses across multiple time frames, including intra-day assessments. Starting in the evening before each operational day, the TSOs use power forecasts and technical constraints of the grid elements to evaluate whether the system will remain secure with respect to current and voltage limits. The increasing share of renewable energy sources, such as solar and wind, has introduced new generation-dominated power flow patterns [6]. These sources are variable, less controllable, and geographically distributed, leading to greater uncertainty in power flows. As a result, the transmission network has become more congested, requiring the system operators

---

\*Corresponding author: jan.viebahn@tennet.eu

to intervene more frequently and operate the grid closer to its physical limits [36]. In many European countries, the pace of renewable capacity additions has outstripped that of grid reinforcement, widening the gap between the grid infrastructure available and the infrastructure needed, and increasing reliance on costly congestion management measures [22, 1]. This trend is expected to continue, putting additional pressure on maintaining grid security and reliability [36].

System operators must balance a range of technical and operational goals that fall under congestion management, including maintaining security margins, meeting time-critical operational requirements, and minimizing costs. This effort leads to a complex decision-making problem characterized by large action spaces, sequential dependencies, uncertainty, and multiple conflicting objectives [40]. In this context, this paper focuses on dynamic grid topology reconfiguration, a sequential decision-making problem in which reconfiguration actions are taken over time in response to evolving grid conditions and operational requirements [39]. Assigning a topology for each hour of a day defines a *topological strategy* (or plan) for the operational day.

Dynamic topology reconfiguration is a practical congestion management measure because it leverages existing infrastructure to influence power flows without requiring new transmission lines. In the congestion management hierarchy, topology switching is classified as a non-costly remedial action, in contrast to redispatching, which requires modifying generation schedules at significant expense [12, 20]. Studies on IEEE test systems have demonstrated that co-optimizing network topology with generation dispatch can yield economic savings of up to 25%, even while maintaining  $N - 1$  reliability standards [19]. In addition to being a cost-effective solution, it can also be implemented in the short term, making it well-suited to address the operational challenges arising from the increasing integration of renewable energy sources. Topology reconfiguration can be achieved by adjusting the connection state of busbar couplers within electrical substations. These couplers act as switches that connect or disconnect busbars, which are the main conductive bars that distribute electricity within a substation. When a busbar coupler is closed, the busbars operate as a single unit, allowing electricity to flow freely between all connected lines and equipment. When the coupler is open, the busbars are electrically isolated, dividing the substation into separate sections with independent connections. This structural change alters how power flows through the network and can be used to relieve overloaded lines. In network topology modeling, this process of separating connected nodes through opening busbar couplers is referred to as *node splitting*.

By adjusting busbar couplers, operators modify the grid topology to relieve overloaded transmission lines. Each line has a maximum allowable current limit, and load flow analysis is used to determine the extent to which this capacity is utilized. These analyses are performed for both normal operating conditions ( $N - 0$ ) and contingency scenarios ( $N - 1$ ), in which a single network element is assumed to fail. In both cases, all transmission lines must remain within their rated limits to ensure system security.

In addition to load flow results, operators consider several other objectives when deciding on topological changes. These include the robustness of the new configuration, that is, how long it remains effective before further switching is required, the total number of switching actions, the structural complexity of the resulting topology in terms of the number of open busbar couplers, and the duration for which an alternative configuration is maintained instead of the default state. A topology change is implemented only if it is expected to improve overall network performance throughout the operational day. This study investigates how topological strategies can be optimized to balance multiple objectives.

Despite the prevalence of heuristics and exact approaches in dynamic topology reconfiguration, a ground-truth benchmark for sequential, multi-objective strategies has not yet been established. Current literature predominantly treats the problem as either a single-objective optimization or a series of independent sub-problems, a simplification largely driven by the perceived computational intractability of evaluating the full combinatorial space over a 24-hour horizon. This lack of exact benchmarks hampers the development and validation of the decision-support tools that transmission system operators increasingly need as congestion management becomes more frequent and more costly [40, 39].

To address this research gap, this paper introduces a unified multi-objective approach that treats the problem as a single global optimization rather than a sequence of independent stages. Two methods are proposed: a brute-force algorithm that systematically evaluates the entire feasible solution space to derive the Pareto front, and an MOEA that searches the solution space heuristically, approximating the Pareto front through iterative variation and selection [13]. The two methods are compared using a

real-world congestion management problem of the TenneT power grid. To evaluate how well the MOEA approximates the true Pareto front, a dedicated evaluation framework is developed using the brute-force solutions as ground-truth reference points. The framework is also suitable for benchmarking algorithms from other studies.

The main contributions of this paper are as follows:

1. We formalize day-ahead transmission topology planning as a sequential multi-objective optimization problem with four operational objectives reflecting real TSO decision criteria.
2. We develop an exact algorithm, named *block algorithm*, that exploits the temporal block structure of strategies to enumerate the complete Pareto front for fixed maximum depth and switch count, computing the solution for a real-world congested day in under three minutes given a precomputed dataset of per-topology load-flow values.
3. We design a tailored MOEA with structure-guided initialization and problem-specific variation operators, and evaluate it against the exact Pareto front using both  $IGD^+$  and a novel multi-front coverage metric.
4. We demonstrate, using real operational data from the Dutch high-voltage grid operated by TenneT, that exact enumeration is not only feasible but outperforms evolutionary search, providing transmission operators with a practical and provably complete decision-support tool.

These contributions are developed and validated across the remainder of the paper as follows: [Section 2](#) reviews the related literature on optimal topology switching and existing optimization frameworks. [Section 3](#) details the problem methodology, establishing the mathematical formulation of the objectives and the proposed algorithms. [Section 4](#) explains the experimental setup and provides an evaluation framework. [Section 5](#) presents experimental results and a performance comparison between block and evolutionary approaches. [Section 6](#) summarizes the key findings of the study, discusses practical implications for grid operators and relevant future research.

## 2 Related Literature

This section reviews the existing literature on optimal topology switching (OTS), the conventional term for the dynamic grid topology reconfiguration problem described above. As grid congestion intensifies with rising renewable penetration, OTS has attracted growing attention as a non-costly remedial action [20, 30].

Although OTS has been extensively studied, the literature encompasses a wide range of problem formulations and modeling assumptions. These differences arise primarily from: (i) the choice of the power flow model, either Alternating Current (AC) or Direct Current (DC) formulation; (ii) the inclusion of additional flexibility options, including dynamic thermal rating (DTR), energy storage systems (ESS), and renewable energy sources (RES); and (iii) the treatment of uncertainty, with data modeled as either deterministic or stochastic [30].

It is worth noting that most OTS studies model switching decisions at the level of transmission lines, whereas the present work focuses on substation reconfiguration through busbar coupler switching (node splitting). Node-breaker formulations that explicitly model substation topology have received comparatively less attention; a notable exception is [21], which formulates OTS at the substation level using a node-breaker representation.

The problem considered in this work adopts a DC load-flow formulation [38], excludes flexibility options, and focuses exclusively on busbar coupler switching decisions (node splitting). All data are assumed to be deterministic.

### 2.1 Classical Optimization Approaches

The foundational work on OTS was introduced by [14], who formulated the problem as a mixed-integer program (MIP) with binary variables representing the status of each transmission element and demonstrated substantial economic savings on the IEEE 118-bus system. Subsequent studies by Hedman

et al. [18, 17] extended this framework to include  $N - 1$  contingency constraints and co-optimization with unit commitment, showing that optimal topology changes can vary from hour to hour while maintaining reliability standards. A review of the economic efficiency and market implications of transmission switching is provided in [19]. More broadly, DC-based OTS problems are predominantly formulated and solved using mixed-integer linear programming (MILP) techniques [30, 31, 32, 27, 3]. The typical objective in these models is to minimize total generation cost, thereby improving operational efficiency through more effective redistribution of power flows. Transmission line thermal limits are explicitly modeled as constraints to ensure network feasibility and security [30].

## 2.2 Topology Optimization using Reinforcement Learning

An alternative line of research addresses grid topology optimization using reinforcement learning (RL). In 2019, the French transmission system operator RTE launched the *Learning to Run a Power Network* (L2RPN) challenge, which stimulated significant interest in applying RL techniques to power network operation and maintenance [29]. Subsequent studies proposed a variety of RL-based solutions, see [37] for a comprehensive overview. Other work explores more advanced AI paradigms. In particular, [12] applied the AlphaZero algorithm, originally developed for complex board games such as chess and Go, to power grid topology optimization. Their results demonstrate a 60% reduction in required redispatching volume, illustrating the potential of topology optimization, despite the high computational and training requirements of such methods.

## 2.3 GridOptions Algorithm

TenneT has also developed its own decision-support tool called *GridOptions*, which incorporates heuristic-based topology optimization methods [39]. The approach uses a dynamic programming algorithm combined with domain-specific heuristics. Initially, load flows are computed for various network topologies using power load and generation forecasts. This list is filtered using a heuristic that prioritizes topologies with the longest congestion-free periods. Finally, a sequential decision graph of network states is built, and strategies are derived using random-weight sampling together with Dijkstra’s algorithm.

The four operational objectives used in the present study (see Section 3.2) were originally identified in the context of GridOptions as key performance metrics for evaluating topological strategies in TenneT’s day-ahead congestion management workflow [39]. However, a head-to-head numerical comparison with GridOptions is outside the scope of this work.

## 2.4 Evolutionary Algorithms

Evolutionary algorithms (EAs) have also been applied to OTS problems. In [15], the OTS problem is solved using a genetic algorithm (GA), a widely used EA for single-objective optimization. Multi-objective evolutionary algorithms (MOEAs) have been employed to address OTS formulations involving competing objectives. In [41], for example, the authors considered both total generation cost and the loss-of-load probability (LOLP), a reliability metric that quantifies the probability of unmet demand over a specified period. Their approach approximated the Pareto front, providing system operators with a set of trade-off solutions balancing cost and reliability.

Beyond OTS, MOEAs, particularly the *Non-dominated Sorting Genetic Algorithm II* (NSGA-II), have been widely applied to combinatorial optimization problems in power systems; for a comprehensive survey see [28]. Because the congestion management problem in this paper involves four competing objectives, it falls into the *many-objective* category, for which the reference-point-based NSGA-III framework [11] has been shown to preserve diversity more effectively than NSGA-II [28]. NSGA-III is therefore adopted as the selection mechanism in the evolutionary algorithm proposed in this work (see Section 3.4).

## 2.5 Exact Methods and Research Gap

To the best of our knowledge, no exact algorithm has been proposed for the multi-objective, sequential formulation of the OTS or dynamic grid topology reconfiguration problem. Existing exact solution approaches rely primarily on mixed-integer optimization formulations that target a single economic objective [14, 32]. In contrast, heuristic and learning-based methods, including reinforcement learning, dynamic programming heuristics, and evolutionary algorithms, are used to obtain approximate solutions with improved scalability but without guarantees of global optimality.

Two important gaps emerge from this literature review. First, the multi-objective nature of operational topology planning (in which system operators must simultaneously balance security margins, switching effort, topological complexity, and deviation from the reference state) has not been addressed through exact methods that can provably enumerate all Pareto-optimal strategies. Second, the sequential structure of the problem, in which a strategy specifies a topology for each hour of the planning horizon, has largely been neglected: most existing methods either optimize a single time step in isolation or aggregate the horizon into a monolithic formulation without exploiting its temporal block structure. The block algorithm introduced in this paper addresses both gaps simultaneously.

## 3 Methodology

This section introduces the mathematical formulation of the congestion management problem and the two proposed solution methods. Section 3.1 defines the fundamental terminology and mathematical notation. Based on these definitions, Section 3.2 formulates the optimization objectives. Finally, Sections 3.3 and 3.4 describe the proposed block algorithm and MOEA, respectively, along with their specific implementations.

### 3.1 Preliminaries

We begin by introducing the terminology and notation used in the rest of the paper.

- We consider a planning horizon consisting of  $T_{\max}$  unit periods. We identify these unit periods with their starting times in  $T := \{0, 1, 2, \dots, T_{\max} - 1\}$ , which we refer to as **time steps**<sup>1</sup>.
- $G_t$  denotes the collection of available network topologies at time step  $t \in T$  (and remains so for the whole following unit period, until the next time step). Each available topology  $g \in G_t$  is described by a heterogeneous graph  $g = (BB(g), BR(g), PO(g), E(g))$ , with node set  $BB(g) \cup BR(g) \cup PO(g)$  and edge set  $E(g)$ , where  $BB(g)$  denotes the set of busbars,  $BR(g)$  the set of transmission branches (i.e., lines and transformers), and  $PO(g)$  includes the set of power injections (i.e., load and generation). The edges in  $E(g)$  represent how the nodes are connected.
- The **reference topology**  $\tilde{g}$  is the graph corresponding to the network configuration with all busbar couplers closed; it is assumed to be available at every time step, i.e.,  $\tilde{g} \in G_t$  for every  $t \in T$ .
- For each time step  $t \in T$ , we consider a set of forecasted power injections. Although stochastic in nature, these are treated as fixed and deterministic parameters during optimization. If topology  $g \in G_t$  is implemented, branch flows are derived using these injections and the DC power flow approximation [38]. For each branch  $b \in BR(g)$ , we denote by  $u_b(g, t)$  the *capacity utilization*, calculated as the ratio of the branch flow to its thermal limit under the worst-case  $N - 1$  contingency scenario. Capacity utilization is expressed as a percentage and may exceed 100% in the event of a line overload.
- For each time step  $t \in T$  and each topology  $g \in G_t$  the worst-case  $N - 1$  line loading is given by

$$LF_1(g, t) := \max_{b \in BR(g)} u_b(g, t).$$

---

<sup>1</sup>In our implementation, we consider a one-day time horizon, with each unit period corresponding to one hour, hence featuring  $|T| = T_{\max} = 24$  time steps. However, the framework presented here is general and can readily be adapted to different time resolutions and time horizons.

- For each topology  $g$ , the *topological depth*

$$d(g) := |BB(g)| - |BB(\tilde{g})|,$$

counts the number of additional busbars created by opening busbar couplers relative to the reference topology  $\tilde{g}$ .

- A *strategy*  $s = (g_t)_{t \in T} \in \mathcal{S}$  is an ordered sequence of topologies, specifying which topology  $g_t \in G_t$  is deployed at each time step  $t \in T$ . The set of all possible strategies is obtained as the Cartesian product of the available topologies across all time steps, that is,  $\mathcal{S} := \times_{t \in T} G_t$ .

### 3.2 Problem objectives

TenneT identified four key performance metrics for evaluating topological strategies [39], all of which we aim to minimize. Specifically, for any strategy  $s = (g_t)_{t \in T} \in \mathcal{S}$ , we consider its:

1. **Worst line capacity utilization in the  $N - 1$  scenario across the entire time horizon:** The first objective seeks to minimize the worst-case network loading across all time steps and all single-line contingencies, that is,

$$LF_1(s) = \max_{t \in T} LF_1(g_t, t);$$

2. **Topological depth across the entire time horizon:** Node splitting increases the network complexity [42], so from the operator perspective, it is convenient to minimize the number of open busbar couplers, motivating the following choice for the second objective:

$$d(s) = \max_{t \in T} d(g_t);$$

3. **Number of topology switches over the entire time horizon:** Switching actions cause mechanical wear on switching assets and carry a small but non-negligible risk of equipment failure or operational error, potentially reducing the system reliability [33]. For this reason, we introduce a third objective to track the number of topology switches required by a strategy as

$$w(s) := \sum_{t \in T \setminus \{0\}} \mathbf{1}_{\{g_t \neq g_{t-1}\}};$$

4. **Utilization of non-reference topologies:** For network operators, it is often desirable to minimize the time spent on network configurations that differ from the reference topology  $\tilde{g}$ , in which all busbars are closed. It is thus natural to formulate a fourth objective as

$$z(s) := \sum_{t \in T} \mathbf{1}_{\{g_t \neq \tilde{g}\}},$$

to count across the time horizon in how many time steps the reference topology  $\tilde{g}$  is not used.

### 3.3 Block algorithm

This subsection introduces the block algorithm, which solves the multi-objective optimization problem defined in Section 3.2. The subsection is structured as follows: Section 3.3.1 provides some preliminary definitions, Section 3.3.2 describes how strategies are retrieved from the block algorithm, Section 3.3.3 explains how the algorithm works, and Section 3.3.4 analyzes the computational complexity of the approach.

### 3.3.1 Preliminary definitions

The key idea behind the block algorithm is that, from an operational perspective, only topology changes matter, not the exact timestamps at which identical topologies persist. By grouping consecutive time steps with identical topologies into blocks, we drastically reduce the effective decision space while preserving exact optimality.

The block algorithm represents strategies by partitioning the time horizon into contiguous, non-overlapping intervals called blocks, during which the network topology remains constant. An available topology is then assigned to each block. This representation aligns naturally with objective 3 (cf. [Section 3.2](#)), which counts the number of topology switches over the time horizon. Formally, a **block**  $B$  is a set of consecutive time steps in  $T$ , specifically

$$B := \{t_s, t_s + 1, \dots, t_e\},$$

for some time steps  $t_s, t_e \in T$  satisfying  $t_s \leq t_e$ . Intuitively,  $t_s$  and  $t_e$  are the indices of the first and last unit periods belonging to  $B$ ; in our hourly setting,  $t_e$  is the index of the (start of the) last hour included. The length  $|B|$  of a block is the number of time steps it comprises, that is,

$$|B| := t_e - t_s + 1.$$

In particular, a block with  $t_s = t_e$  has length one and represents a single unit period. For a given collection  $T$  of time steps, let  $\mathcal{B}$  be the resulting collection of all possible blocks. Two blocks  $B, B' \in \mathcal{B}$  are said to be consecutive if  $B'$  begins with the unit period immediately following the last unit period included in  $B$ , i.e., if  $t_s(B') = t_e(B) + 1$ .

A **block configuration** is a finite collection  $M$  of blocks  $M := \{B_1, B_2, \dots, B_{|M|}\}$  that satisfies the following two conditions:

- **Non-overlapping blocks:**  $B_i \cap B_j = \emptyset$  for every  $1 \leq i < j \leq |M|$ ;

- **Coverage of the entire horizon:**  $\bigcup_{i=1}^{|M|} B_i = T = \{0, 1, \dots, T_{\max} - 1\}$ .

Let  $\mathcal{M}(l)$  be the set of all block configurations with  $l + 1$  blocks, that is

$$\mathcal{M}(l) := \{M \subseteq \mathcal{B} : M \text{ is a block configuration and } |M| = l + 1\}. \quad (1)$$

Each configuration in  $\mathcal{M}(l)$  partitions  $T$  into  $l + 1$  consecutive blocks.

We now extend the notation and definitions introduced in [Sections 3.1](#) and [3.2](#) to also work with blocks and block configurations.

The set of topologies always available within a block  $B$  is

$$G_B := \bigcap_{t \in B} G_t.$$

Motivated by objective 1 in [Section 3.2](#), we define the best-case load flow across block  $B$  for a constant topology in some  $G \subseteq G_B$  as

$$LF_1(B, G) := \min_{g \in G} \max_{t \in B} LF_1(g, t),$$

with the assumption that if the second argument is omitted, then the minimum is taken over  $G_B$ , i.e., over all the topologies available in that block  $B$ , i.e.,

$$LF_1(B) := LF_1(B, G_B).$$

A natural subset of topologies available in block  $B$  to which we might want to restrict is the subset  $G_B^{(\leq d)}$  of topologies available in block  $B$  that have a topological depth at most  $d$ , i.e.,

$$G_B^{(\leq d)} := \{g \in G_B : d(g) \leq d\} \subseteq G_B.$$

This is particularly relevant when working with objective 2 in [Section 3.2](#). Indeed, it is often interesting to calculate the best achievable  $LF_1$  metric for a given block  $B$  with available topologies restricted to having a depth not larger than a target  $d$ , for which we introduce the notation

$$LF_1(B, d) := LF_1(B, G_B^{(\leq d)}).$$

The notation for best achievable  $LF_1$  metrics can be trivially extended from blocks to block configurations, namely

$$LF_1(M) := \max_{B \in M} LF_1(B)$$

is the best achievable  $LF_1$  for a block configuration  $M$ , and

$$LF_1(M, d) := \max_{B \in M} LF_1(B, d) \quad (2)$$

is the best achievable  $LF_1$  for a block configuration  $M$  restricted to topologies of depth at most  $d$ .

A strategy  $s \in S$  can be equivalently described by specifying the blocks in which the topology prescribed by  $s$  does not change and the corresponding topology associated with each block. Given a strategy  $s = (g_t)_{t \in T} \in S$  and a block  $B$ , we write  $s|_B = g$  for some  $g \in G_B$  if  $g_t = g$  for all time steps  $t \in B$  (and the corresponding unit periods they represent).

Related to objective 3 in [Section 3.2](#), we can associate with each block configuration  $M$  the subset of strategies  $S(M)$  that have a constant topology during each block  $B \in M$ , i.e.,

$$S(M) := \{s \in S : s|_B = g \text{ for some } g \in G_B \forall B \in M\}.$$

It is easier to describe strategies in  $S(M)$  because we just need to specify one topology for each block  $B \in M$  rather than one topology for each time step  $t \in T$ . We assume that all strategies in  $S(M)$  have distinct topologies on consecutive blocks, so that the number of switching time steps for any strategy in  $S(M)$  is equal to  $|M| - 1$  by construction, since it is determined by the number of blocks in  $M$ . We formally define the auxiliary function  $w(M)$  as

$$w(M) := |M| - 1,$$

which extends the already introduced notation  $w(\cdot)$  for strategies directly to blocks.

Finally, since objective 4 in [Section 3.2](#) aims to minimize the utilization of non-reference topologies, it is convenient to track explicitly which blocks are assigned the reference topology. For this reason, given a block configuration  $M = \{B_1, \dots, B_{|M|}\}$ , we denote by  $\mathcal{A}(M)$  the collection of all possible combinations of non-consecutive blocks in  $M$

$$\mathcal{A}(M) := \left\{ R \subseteq M : \forall B, B' \in R : t_s(B) \neq t_e(B') + 1, t_s(B') \neq t_e(B) + 1 \right\}. \quad (3)$$

Note that the configurations in  $\mathcal{A}(M)$  are not block configurations themselves since, by construction, they do not cover the entire time horizon.

The set of strategies that use a specific block configuration  $M$  can be further partitioned depending on the blocks in which the reference strategy  $\tilde{g}$  is used. Specifically, for every  $R \in \mathcal{A}(M)$ , we define the subset of strategies

$$S(M, R) := \{s \in S(M) : s|_B = \tilde{g} \forall B \in R\}$$

for which the utilization of the reference topology is explicit in all the blocks in  $R$ . Note that, given that  $\tilde{g} \in G_t$  for all  $t \in T$  (as noted in [Section 3.1](#)), it follows by definition that  $\tilde{g} \in G_B$  for every block  $B \in \mathcal{B}$ .

Naturally, the number  $z(s)$  of time steps for which the reference topology is used for any strategy  $s \in S(M, R)$  is entirely determined by the blocks in  $R$ , which justifies the following notation

$$z(R) := \sum_{B \in R} |B|.$$

Given a triplet  $(d, M, R)$ , we denote by  $LF_1(d, M, R)$  the best achievable  $LF_1$  given a block configuration  $M$ , a reference block assignment  $R$ , and topologies having a maximum topological depth of  $d$ . In symbols,

$$LF_1(d, M, R) := \max \left\{ \max_{B \in M \setminus R} LF_1(B, G_B^{(\leq d)}), \max_{B \in R} LF_1(B, \{\tilde{g}\}) \right\},$$

extending [Eq. \(2\)](#).

### 3.3.2 Deriving Feasible Strategies

Given a block configuration  $M$ , we want to determine the corresponding strategies, i.e., the specific topologies at each time step that produce the evaluated objective values. We achieve this through a final filtering step that restricts the available topologies in each block  $B$  to those that satisfy both the topological depth and  $LF_1$  threshold.

The set of feasible strategies associated with a configuration  $(d, M, R)$  is defined as the Cartesian product over all active (non-reference) blocks:

$$\mathcal{S}(d, M, R) := \left\{ s = ((g_B)_{B \in M \setminus R}, (\tilde{g}_B)_{B \in R}) : d(g_B) \leq d, \max_{t \in B} LF_1(g_B, t) \leq LF_1(d, M, R) \forall B \in M \setminus R \right\}. \quad (4)$$

Each strategy  $s \in \mathcal{S}(d, M, R)$  specifies a feasible combination of topologies having the objective values  $(d, w(M), z(R), LF_1(d, M, R))$ .

### 3.3.3 Logic of block algorithm

We now present the block algorithm, whose pseudocode is given in [Algorithm 1](#) using the definitions from [Section 3.3.1](#). The algorithm takes as input a maximum topological depth  $d^{\max}$  and a maximum number of switching time steps  $s^{\max}$ , and systematically enumerates all combinations of block configurations  $M$ , reference topology assignments  $R$ , and depth levels  $d$  to identify the complete set of nondominated configurations with respect to the objectives defined in [Section 3.2](#). The main steps are as follows:

- First, an empty set  $C$  of objective values is initialized. Then we loop through each possible depth level from 0 to  $d^{\max}$ .
- Second, for each number of switching time steps  $l$  between 0 and  $s^{\max}$ , we consider every possible block configuration  $M \in \mathcal{M}(l)$ .
- For each block configuration  $M$ , all reference topology assignments  $R \in \mathcal{A}(M)$  are evaluated. Subsequently, for each combination  $(d, M, R)$  the objective values  $(d, w(M), z(R), LF_1(M, R, d))$  are calculated and appended to  $C$ .
- Once all objective values have been calculated, the set  $C$  is filtered using a nondominated sorting procedure as explained in [Algorithm 2](#), resulting in a new subset  $C^*$ , which is then returned as output.

---

#### Algorithm 1 BlockAlgorithm

---

**Require:** Maximum topological depth  $d^{\max}$ , maximum number of switching time steps  $s^{\max}$

▷ Initialize set of objective values:

```

1:  $C \leftarrow \emptyset$ 
2: for  $d = 0 \rightarrow d^{\max}$  do
3:   for  $l = 0 \rightarrow s^{\max}$  do
4:     ▷ Loop through every block configuration  $M$ :
5:     for  $M \in \mathcal{M}(l)$  do
6:       ▷ Loop through every possible reference topology assignment  $R$ :
7:       for  $R \in \mathcal{A}(M)$  do
8:         ▷ Append objective values to set  $C$ :
9:          $C \leftarrow C \cup (d, M, R, w(M), z(R), LF_1(d, M, R))$ 
10:      end for
11:    end for
12:  end for
13:  ▷ Filter nondominated configurations using Algorithm 2:
14:   $C^* \leftarrow \text{FilterNonDominated}(C)$ 
15: return  $C^*$ 

```

---

Each element of  $C^*$  corresponds to at least one feasible strategy that is Pareto-optimal with respect to the four objectives. This subset is determined from  $C$  by [Algorithm 2](#), which is a custom nondominated sorting algorithm that leverages the fact that all objective functions except  $LF_1$  take finite integer values. More precisely, non-dominated solutions can be easily identified by comparing the  $LF_1$  values between neighbors in the dimensions of the discrete objectives (see lines 4-15 in [Algorithm 2](#)). This approach identifies nondominated solutions more efficiently than conventional sorting methods.

---

**Algorithm 2** FilterNonDominated

---

**Require:** Set of objective values  $C$ , maximum depth  $d^{\max}$ , maximum number of switching time steps  $s^{\max}$ , and set of time steps  $T$ .

▷ Initialize the tensor  $O$  by setting all elements to infinity. A padding of  $-1$  is added so that neighbor lookups are well-defined and do not require specific boundary cases.

1:  $O_{d,l,n} \leftarrow \infty \quad \forall d \in \{-1, 0, \dots, d^{\max}\}, \quad \forall l \in \{-1, 0, \dots, s^{\max}\}, \quad \forall n \in \{-1, 0, \dots, T_{\max}\}$

▷ For all indices, update  $O_{d,l,n}$  with the minimum load flow value  $LF_1(d, M, R)$  for each  $(d, w(M), z(R))$  from the set  $C$ :

2:  $O_{d,l,n} \leftarrow \min\{LF_1(d, M, R) : (d, M, R, w(M), z(R), LF_1(d, M, R)) \in C, w(M) = l, z(R) = n\}$

▷ Initialize  $R^{nds}$  as an empty collection of non-dominated solutions:

3:  $R^{nds} \leftarrow \emptyset$

▷ Iterate over all elements in the tensor  $O$ :

4: **for**  $d = 0 \rightarrow d^{\max}$  **do**

5:     **for**  $l = 0 \rightarrow s^{\max}$  **do**

6:         **for**  $n = 0 \rightarrow T_{\max}$  **do**

        ▷ Determine the minimum  $LF_1$  value from neighboring elements:

7:              $LF_1^{nb} \leftarrow \min\{O_{d-1,l,n}, O_{d,l-1,n}, O_{d,l,n-1}\}$

        ▷ Compare the current  $LF_1$  value after rounding to the first decimal place

8:             **if**  $\text{round}(O_{d,l,n}) < \text{round}(LF_1^{nb})$  **then**

               ▷ Store the current  $LF_1$  value if it is lower than its neighboring values:

9:                  $R^{nds} \leftarrow R^{nds} \cup \{(d, l, n, O_{d,l,n})\}$

10:             **else**

               ▷ Otherwise, update the current value to the best neighboring  $LF_1$  value:

11:                  $O_{d,l,n} \leftarrow LF_1^{nb}$

12:             **end if**

13:         **end for**

14:     **end for**

15: **end for**

16: **return**  $R^{nds}$

---

The rounding in line 8 of [Algorithm 2](#) is applied to the first decimal place to avoid distinguishing solutions whose  $LF_1$  values differ by less than 0.1. This ensures that the nondominated sorting reflects operationally meaningful differences rather than numerical noise.

### 3.3.4 Computational complexity of the block algorithm

The tractability of the block algorithm rests on two observations: the number of distinct ways in which the time horizon can be partitioned into blocks is relatively small (as we quantify below), and three of the four objectives take discrete integer values, which allows efficient nondominated sorting. Together, these properties enable the algorithm to pre-compute and store all relevant objective values for each block and to enumerate the complete Pareto front in polynomial time for fixed operational bounds on depth and switch count. We now make this precise by analyzing the computational complexity of the block algorithm in detail.

A block  $B$  is uniquely determined by its starting point  $t_s$  and its end point  $t_e$  from  $T$ . Therefore, the total number of unique blocks is equal to the number of ways to choose two distinct time steps from  $|T| = T_{\max}$  available options, which is given by  $\binom{T_{\max}}{2}$ , plus the  $|T_{\max}|$  blocks of length 1, for which  $t_s = t_e$ . In our experimental setting, we will work with a one-day time horizon, subdivided into

$T_{\max} = 24$  unit periods, each representing an hour. For this choice, the total number of distinct blocks is quite modest and equal to  $|\mathcal{B}| = \binom{24}{2} + 24 = 300$ , allowing us to pre-compute and store all objective values in [Section 3.2](#) for each block.

As described in [Section 3.3.3](#), the algorithm iterates through every possible combination of  $d$ ,  $M$ , and  $R$ , corresponding to a maximum topology depth, block configuration, and set of reference block assignments. The number of iterations is therefore based on the following components:

- The number of possible block configurations.
- The number of possible reference topology assignments given a block configuration.
- The number of depth values considered.

In the following paragraphs, we examine in detail how each component contributes to the total number of iterations required to find all solutions.

The total number of block configurations depends on the number of possible switching time steps. Assuming we start with a block at time step  $t = 0$ , there are  $T_{\max} - 1$  potential switching time steps within the time horizon. At each time step, there are two possibilities: start a new block or “extend” the current block. As a result, the total number of block configurations is equal to  $2^{T_{\max}-1}$ . Many of the resulting block configurations prescribe a large number of switching actions, possibly even at every time step. In practice, however, we are interested in configurations with a limited number of switches, in line with objective 3 in [Section 3.2](#).

For any  $l \in \{0, T_{\max} - 1\}$ , let  $p(l)$  be the number of block configurations with exactly  $l$  switching time steps and thus consisting of exactly  $l + 1$  blocks, which is equal to

$$p(l) := \binom{T_{\max} - 1}{l}. \quad (5)$$

Consequently, the number of block configurations with at most  $l$  switches is given by

$$P(l) := \sum_{i=0}^l p(i) = \sum_{i=0}^l \binom{T_{\max} - 1}{i}. \quad (6)$$

Note that calculating  $P(T_{\max} - 1)$ , we recover  $2^{T_{\max}-1}$ , which is the total number of block configurations.

Next, we consider the number of possible reference-topology assignments for a given block configuration. In each block  $B \in M$ , we can either use the reference topology or not. Consequently, the total number of ways to assign the reference topology blocks to a configuration  $M$  is equal to  $2^{|M|}$ . However, the number of possibilities to evaluate can be reduced by considering only combinations in which no two consecutive (connected) blocks are selected as reference blocks, as explained below.

We say that two consecutive blocks,  $B_i$  and  $B_{i+1} \in M$ , are *connected* if the end point of  $B_i$  directly precedes the start point of  $B_{i+1}$ , that is, if  $t_{e_i} + 1 = t_{s_{i+1}}$ . Suppose both connected blocks are selected as reference blocks. In that case, the block configuration  $M$  is equivalent to the configuration  $M'$  obtained by replacing  $B_i$  and  $B_{i+1}$  with a single reference block  $B^* = B_i \cup B_{i+1} = \{t_{s_i}, \dots, t_{e_{i+1}}\}$ . Selecting  $B_i$  and  $B_{i+1}$  together or selecting the merged block  $B^*$ , yields the same total number of time steps assigned to the reference topology,

$$z(R) = z(R'),$$

and the same  $LF_1$  value,

$$LF_1(M, R, d) = LF_1(M', R', d),$$

where  $R' = (R \setminus \{B_i, B_{i+1}\}) \cup \{B^*\}$ .

The block algorithm processes configurations in increasing order of  $|M|$ ; that is, it first evaluates all configurations consisting of a single block, then all configurations with two blocks, and so on. Since  $M'$  contains one fewer block than  $M$ , i.e.,  $|M'| = |M| - 1$ , this reduced configuration corresponds to a case that has already been evaluated in an earlier iteration of the algorithm and therefore does not need to be reevaluated.

The number of feasible reference assignments for a configuration with  $N = |M|$  blocks, defined by  $\mathcal{A}(M)$  in Eq. (3), corresponds to the number of subsets  $\{1, \dots, N\}$  that contain no consecutive indices. It is well known in combinatorics that this quantity follows the Fibonacci recurrence,

$$f(N) = f(N - 1) + f(N - 2),$$

with initial conditions  $f(1) = 2$  and  $f(2) = 3$ . Thus, the number of possible reference assignments grows according to the Fibonacci sequence,

$$f(N) = F_{N+2},$$

(see, e.g., [35, 2]).

The final component of the computational complexity concerns depth. For each block configuration  $M$ , the algorithm iteratively filters the topology sets  $G_B$  for all  $B \in M$  across depth levels  $d = 1, 2, \dots, d^{\max}$ . At each depth level, only the filtered subsets  $G_B^{(\leq d)}$  are retained, and the corresponding  $LF_1$  for the block configuration and each block reference assignment needs to be reevaluated.

Knowing the computational complexity of each component, we can express the total number of iterations required for a given time horizon, maximum depth, and maximum number of switches (equivalently, a maximum number of blocks minus one) using the following equation:

$$N_{\text{eval}}(d^{\max}, l^{\max}, T_{\max}) = d^{\max} \cdot \sum_{l=0}^{l^{\max}} \binom{T_{\max} - 1}{l} F_{l+2}, \quad (7)$$

where  $d^{\max}$  and  $l^{\max}$  denote the maximum depth and switches, respectively.

The total number of evaluations grows linearly with  $d^{\max}$  and polynomially with  $T_{\max}$  of degree  $l^{\max}$ , leading to an overall complexity of  $\mathcal{O}(d^{\max} T_{\max}^{l^{\max}})$ .

In practice,  $d^{\max}$  and  $l^{\max}$  are small constants determined by operational constraints, meaning the algorithm scales polynomially with the number of timesteps (polynomially for fixed operational bounds on depth and switch count) and remains computationally tractable for realistic problem sizes. If  $l^{\max}$  were allowed to increase with  $T_{\max}$ , the complexity would become exponential, but such configurations are not relevant for operational use cases.

### 3.4 Multi-objective evolutionary algorithm (MOEA) framework

This section describes a multi-objective evolutionary algorithm (MOEA) tailored to the congestion management problem defined in Section 3.2. An evolutionary algorithm maintains a population of candidate solutions (chromosomes), which are iteratively improved through selection, crossover, and mutation until a termination criterion is met [13]. The following subsections detail how each component (representation, initialization, variation, and selection) is adapted to the specific structure of the topology planning problem.

#### 3.4.1 Representation

In an evolutionary algorithm, each candidate solution is encoded as a chromosome (genotype); the mapping to the actual decision variables (phenotype) determines how genetic operators translate into meaningful changes [13]. Our choice of chromosome formulation is guided by [4], which evaluates three representation schemes for multi-objective sequential decision problems: direct variable-length encoding, integer-valued priority-based encoding, and random-key-based encoding. Their empirical comparison shows that random-key-based encoding yields the strongest overall performance across multigraph shortest-path instances, owing to its flexibility and favorable search dynamics. However, for the congestion problem introduced in Section 3.2, this approach becomes impractical. In our setting, each gene must encode a topology–time pair, implying a chromosome length of

$$\sum_{t \in T} |G_t|,$$

which can quickly get very large in our setting. Such long chromosomes incur high memory costs and increased runtime in both variation and evaluation. The same issue arises with the integer-valued priority-based representation, whose length scales in the same way, rendering it similarly unsuitable for our

problem structure. Direct variable-length encoding is therefore the natural choice. In this representation, the number of genes scales directly with the number of time steps, resulting in compact chromosomes and efficient operator application. An additional advantage is the one-to-one correspondence between genotype and phenotype: each chromosome encodes a unique solution trajectory. The authors in [4] highlight that this bijectivity avoids search-space plateaus that arise in one-to-many encodings, where multiple genotypes correspond to the same phenotype and therefore share identical fitness values, reducing search efficiency.

A commonly cited drawback of direct variable-length encoding is the potential formation of loops when applying crossover or mutation, which may require explicit repair procedures to restore feasibility [4]. In our setting, however, loop formation is structurally impossible. A solution consists of a topology sequence  $s = (g_t)_{t \in T}$ , where each topology corresponds to a distinct time step. Transitions are allowed only from one time step to the next and never to a previous or current time step. Therefore, the problem’s structure prevents loops by design. For these reasons, direct variable-length encoding has been adopted as the chromosome representation.

### 3.4.2 Initial Population

Before the evolutionary process begins, the initial population must be generated. There are two main prerequisites for this population: each chromosome must encode a feasible strategy, and the solutions should be sufficiently diverse within the objective space. Diversity in the initial population improves coverage of the search landscape, enabling evolutionary operators to explore multiple promising regions and reducing the risk of premature convergence [13].

A straightforward approach is random initialization, which in our setting amounts to independently selecting a topology  $g_t \in G_t$  uniformly at random for each time step  $t \in T$ . While simple, this method performs poorly for our problem for two structural reasons:

- **Skewed topological depth distribution.** By construction, the set  $G_t$  of available topologies at time step  $t$  contains substantially more topologies with a large topological depth. Uniform random sampling is therefore unlikely to generate strategies with small depth values, which are preferable since one of the main objectives (see Section 3.2) is to minimize the maximum topological depth along a strategy.
- **Excessive number of switches.** Combining topologies independently sampled for each time step  $t$  tends to produce strategies with many switches, far more than would occur in realistic or high-quality solutions.

As a consequence, a uniform random initialization yields a population that is diverse in its raw encodings but not diverse in the relevant objective-space dimensions (number of switches and depth). This hinders the chosen evolutionary algorithm’s ability to produce a high-quality approximation of the Pareto front. To address this limitation, we design a custom sampling procedure that systematically balances diversity across these structural properties of strategies.

Structure-Guided Sampling Based on Switch Count. For any given switch count  $l$ , we first select a random subset of block configurations  $\mathcal{M}'(l) \subset \mathcal{M}(l)$ , defined earlier in Eq. (1). For each block configuration  $M \in \mathcal{M}'(l)$ , we consider its blocks  $B \in M$  and for each block  $B$  we draw one topology at random from the corresponding topology collection  $G_B$ . This procedure generates strategies that share the same number of switches  $l$  but differ in their switching locations and topology choices. Formally, the set of all possible strategies with exactly  $l$  switches is

$$\mathcal{S}^{(l)} := \bigcup_{M \in \mathcal{M}'(l)} \{s = (g_B)_{B \in M} : g_B \in G_B, \forall B \in M\},$$

from which we sample a finite subset  $\mathcal{P}^{(l)} \subset \mathcal{S}^{(l)}$ . The switch-based component of the initial population is then obtained by merging all these subsets into

$$\mathcal{P}_l = \bigcup_{l=0}^{l_{\max}} \mathcal{P}^{(l)}.$$

This ensures that the initial population contains strategies spanning a broad yet well-controlled number of switches.

Structure-Guided Sampling Based on Depth. To introduce diversity for the maximum depth objective, we similarly generate strategies associated with controlled maximum depth values. The depth-based component of the initial population is defined as

$$\mathcal{P}_d = \bigcup_{d=0}^{d^{\max}} \mathcal{P}^{(d)},$$

where  $\mathcal{P}^{(d)}$  is a random subset of feasible strategies whose maximum depth is exactly equal to  $d$ . Because the depth of a strategy is determined after sampling, a small number of sampled strategies may achieve depth values lower than the target depth  $d$ . These outliers are removed and resampled to maintain the intended distribution across depth levels.

The final initial population combines diversity across both switch count and maximum depth via

$$\mathcal{P} = \mathcal{P}_l \cup \mathcal{P}_d.$$

Structure-Guided Sampling Sizes. The sizes of the individual subsets used to construct the initial population are controlled by two predefined sampling parameters, denoted by  $\bar{l}$  and  $\bar{d}$ . Specifically, for the switch-based sampling, each subset  $\mathcal{P}^{(l)}$  associated with a switch count  $l$  is sampled with fixed cardinality

$$|\mathcal{P}^{(l)}| = \bar{l}, \quad \forall l \in \{0, \dots, T\}.$$

Similarly, for the depth-based sampling, each subset  $\mathcal{P}^{(d)}$  associated with a target maximum depth  $d$  is sampled with fixed cardinality

$$|\mathcal{P}^{(d)}| = \bar{d}, \quad \forall d \in \{1, \dots, d^{\max}\}.$$

Note that for  $d = 0$  is excluded from this sampling procedure, since there is a unique topology at that depth, i.e., the reference topology  $\tilde{g}$ , which is always added to the initial population.

Parameters  $\bar{l}$  and  $\bar{d}$  directly determine the contribution of the switch-based and depth-based components to the total population size  $\mathcal{P}$ , yielding

$$|\mathcal{P}| = T_{\max} \cdot \bar{l} + d^{\max} \cdot \bar{d} + 1. \quad (8)$$

This construction yields an initial population that is (i) composed exclusively of feasible strategies and (ii) explicitly diverse in the objective-space dimensions that govern search difficulty. As a result, it provides a more informative and balanced starting point for the MOEA than uniform random sampling, thereby improving its exploratory capabilities and overall optimization performance.

### 3.4.3 Variation: Crossover and Mutation

This subsection describes the variation operators, crossover, and mutation, used in the proposed MOEA algorithm. Variation operators are central to evolutionary algorithms: crossover primarily supports exploitation by recombining favorable genetic material from parent solutions, whereas mutation promotes exploration by introducing stochastic perturbations that enable the discovery of novel regions of the search space. A key design requirement for the variation operators is that the resulting offspring remain feasible. Recall that at each time step  $t$ , only a restricted collection  $G_t$  of topologies is available. A chromosome encodes a strategy  $s = (g_t)_{t \in T}$  subject to the constraint that each gene satisfies  $g_t \in G_t$  for all  $t \in T$ . Any variation operator must therefore ensure that this constraint is satisfied by all offspring.

A crossover method that ensures this feasibility is the *k-point crossover operator*. In this operator,  $k$  crossover points are selected uniformly at random along the chromosome, partitioning it into  $k + 1$  contiguous segments. The offspring's chromosomes are then formed by alternately copying segments from the two parents. Crucially, because each gene position  $t$  in the offspring is copied from the corresponding position in one of the parents, and both parents satisfy  $g_t \in G_t$ , feasibility is preserved by construction.

Beyond feasibility preservation, the choice of  $k$ -point crossover is further motivated by the temporal structure of the decision horizon. For example, in uniform crossover, where the allele at each time step is selected independently from either parent, the recombination process introduces many topology changes in the offspring. As a result, contiguous temporal patterns present in the parents become frequently fragmented. In contrast,  $k$ -point crossover preserves contiguous temporal segments of the chromosome, thereby maintaining the integrity of temporal sequences inherited from the parents. This results in fewer disruptions of temporal structure, so offspring tend to retain effective switching patterns. In conclusion,  $k$ -point crossover provides a simple and widely used recombination mechanism that respects temporal coherence while preserving feasibility, without introducing additional problem-specific assumptions or implementation complexity.

Mutation is implemented via a *random-reset operator*. Each gene  $g_t$  is independently selected for mutation with probability  $p_m$ . If a mutation occurs at time step  $t$ , the current gene is replaced by a new topology sampled uniformly at random from the set  $G_t$ . Since all possible replacements are in  $G_t$ , this operator also ensures feasibility.

### 3.4.4 Evaluation and Selection

The evaluation and selection mechanisms jointly drive the evolutionary search toward high-quality solutions. Evaluation assigns fitness values to chromosomes based on their performance with respect to the problem objectives, while selection determines which individuals are retained and propagated to subsequent generations.

The objective functions defined in [Section 3.2](#) are used directly as fitness functions, which is possible because the genotype and phenotype coincide for the chosen direct encoding (see [Section 3.4.1](#)). Selection must balance convergence toward high-quality solutions with diversity preservation across four competing objectives.

Since this qualifies as a many-objective problem, we adopt the NSGA-III framework [11], which extends the classical NSGA-II framework by combining nondominated sorting with reference-point-based diversity preservation.

In nondominated sorting, solutions are ranked into successive fronts based on Pareto dominance: the first front contains all solutions that are not dominated by any other solution, the second front contains solutions dominated only by those in the first front, and so on.

This approach does not require any weighting schemas and thus avoids objective aggregation, treating all objectives equally. Moreover, the explicit Pareto-ranking structure of NSGA-III facilitates the interpretability of the trade-offs among competing objectives. From a computational perspective, NSGA-III has the same asymptotic per-generation complexity as NSGA-II, with only minor additional overhead due to reference-point association.

NSGA-III has been shown to outperform MOEA/D [5], IBEA [43], and MOPSO [7, 8] on combinatorial many-objective benchmarks [28]. In view of all these considerations, NSGA-III is adopted as the selection algorithm in this study.

## 4 Experimental Setup

This section outlines the experimental setup used to evaluate and compare the performance of the proposed MOEA. We first introduce the dataset and its construction in [Section 4.1](#). The choice of hyperparameters and the experimental protocol are detailed in [Section 4.2](#). Finally, we introduce the evaluation metrics used to assess the MOEA’s effectiveness against the block algorithm’s exact solutions in [Section 4.3](#).

### 4.1 Dataset

To obtain a transparent and computationally efficient evaluation, we decouple the power grid calculations from the optimization process by constructing an offline dataset. For each time step, this dataset contains the set of available topologies together with their associated congestion-related metrics, defining the complete search space explored by both the block and evolutionary algorithms.

The dataset is derived from real-world operational data from TenneT and represents a portion of the Dutch high-voltage transmission grid. All load-flow calculations are based on a single operational day selected for its high network congestion. As shown in Table 1, the  $LF_1$  values of the reference topology exceed 100% for the majority of time steps, with peaks above 125% during the evening hours ( $t = 18-20$ ), indicating severe overloading under  $N-1$  contingency conditions. This day therefore represents stressed operating conditions in which topology-based congestion management is most critical.

To enable efficient large-scale evaluation, active power flows are computed using the DC approximation [38], a standard linearization that assumes small angle differences, flat voltage profiles, negligible line resistance, and lossless transmission. While less accurate than full AC models, the DC approximation is widely used in transmission-level studies and provides a favorable trade-off between computational efficiency and modeling fidelity. In particular, it allows the repeated evaluation of hundreds of thousands of candidate topologies, which would be computationally infeasible using full AC power flow within a brute-force or evolutionary optimization loop.

Using DC power flow calculations, the capacity utilization  $LF_1(g, t)$  and topological depth  $d(g)$  are computed for all available topologies at each time step, as defined in Section 3.1. The selected day comprises a total of 252,094 unique topologies. Table 1 reports the count  $|G_t|$  of available topologies per time step, together with the  $LF_1$  value of the reference topology ( $LF_1(\tilde{g})$ ).

Time step $t$	0	1	2	3	4	5	6
$ G_t $	39180	39180	39180	39180	39180	39180	39180
$LF_1(\tilde{g})$	112.0	100.0	101.4	104.2	106.0	113.6	144.4
Time step $t$	7	8	9	10	11	12	13
$ G_t $	19950	19590	19590	19590	19590	19590	19590
$LF_1(\tilde{g})$	119.8	126.2	120.0	115.6	118.0	118.8	113.3
Time step $t$	14	15	16	17	18	19	20
$ G_t $	19590	19590	19590	19590	19590	19590	19590
$LF_1(\tilde{g})$	101.4	103.2	102.4	111.6	128.9	142.1	136.7
Time step $t$	21	22	23				
$ G_t $	39180	39180	39180				
$LF_1(\tilde{g})$	131.1	123.6	113.3				

Table 1: Number of available topologies  $|G_t|$  and the load flow value of the reference topology ( $LF_1(\tilde{g})$ ) for each time step  $t \in T$ .

The distribution of topological depths across the dataset is summarized in Table 2. The dataset is highly imbalanced, with the majority of available topologies concentrated at depth 3.

Topological depth	# of topologies
0	1
1	489
2	20777
3	230827

Table 2: Number of unique available topologies at each depth  $d = 0, 1, 2, 3$  in the dataset.

## 4.2 Hyperparameters for MOEA

The proposed MOEA is inherently stochastic, so each experimental configuration is evaluated over 15 independent random seeds. Since the runs are independent, they are executed in parallel without increasing wall-clock time.

To assess the algorithm’s robustness and sensitivity to key design choices, several hyperparameter configurations are considered. The experimental variations focus on three central parameters: population

size, crossover probability  $p_c$ , and mutation probability  $p_m$ . In all configurations, the crossover and mutation probabilities are set as complements,  $p_c = 1 - p_m$ , so that the experimental variations effectively reduce to a single parameter. Note that  $p_c$  governs whether crossover is applied to a selected pair of parents, while  $p_m$  is the per-gene probability of random reset; the two operators act at different levels and their complementary coupling is a design choice rather than a theoretical requirement. All remaining algorithmic components are kept fixed across experiments to isolate the effects of these parameters. Evaluating multiple hyperparameter combinations across several random seeds increases the likelihood of obtaining a well-distributed and high-quality approximation of the Pareto front. [Table 3](#) summarizes the algorithmic settings that are fixed in all experiments.

Parameter	Value/choice
Seeds	15
Crossover method	$k$ -point crossover, with $k = 2$
Mutation method	Random reset
Selection method	NSGA-III
Reference directions	100
Termination	30 minutes

Table 3: Standard algorithm configurations

One requirement for NSGA-III is the reference directions. The reference directions are uniformly distributed across the normalized action space and are generated using a Riesz  $s$ -energy minimization approach [16]. For the four-objective problem, 100 reference directions are used, as this number provides sufficiently fine coverage of the normalized objective space while remaining compatible with the chosen population sizes.

All experiments are run on a Microsoft Dev Box virtual machine equipped with 32 GB of RAM and a 64-core processor (2.44 GHz). The block algorithm described in [Section 3.3](#) computes the full Pareto front for a problem instance of the considered size in under 3 minutes. To ensure that the evolutionary algorithm is not constrained by limited runtime and has ample opportunity to explore the search space, each MOEA run is allocated a substantially larger computational budget of 30 minutes. Note that, given a fixed time budget, mutation and crossover probabilities have no significant effect on the number of generations; only the population size does.

The first configuration-specific hyperparameter is the population size, which strongly influences the balance between exploration and convergence. Smaller populations allow more generations to be completed within a fixed time budget, increasing the frequency of crossover and mutation events, and enabling faster short-term adaptation. However, they may suffer from limited diversity and a higher risk of premature convergence. Larger populations preserve greater genetic diversity and improve coverage of the Pareto front, but typically evolve more slowly because fewer generations can be completed. To examine this trade-off, experiments are conducted using small (**S**), medium (**M**), and large (**L**) population sizes.

Each population size is determined by the sampling parameters  $\bar{l}$  and  $\bar{d}$  introduced in [Section 3.4.2](#). For configuration **S**, the sampling parameters  $\bar{l}$  and  $\bar{d}$  are both set to 30, yielding an initial population of 811 individuals. We note that, in this way, the population size is set to be an order of magnitude higher than the number of solution points found by the block algorithm (83 in total, as detailed later in [Table 7](#)), hence giving the MOEA a fair chance to discover all these optimal solutions. The parameters  $\bar{l}$  and  $\bar{d}$  are linearly scaled and set to 45 for configuration **M** and 60 for configuration **L**. This results in total population sizes of 1,216 and 1,621, respectively, as summarized in [Table 4](#).

For each hyperparameter configuration, we run 15 independent evolutionary runs in parallel, each with a different seed. Although the termination criterion is time-based in principle, in order to get comparable results across different seeds, individual runs are, in practice, terminated after a fixed number of generations, as detailed below in [Table 4](#).

In addition to population size, the mutation and crossover probabilities directly influence the balance between exploration and exploitation in the evolutionary process. Mutation introduces stochastic perturbations that promote exploration of previously unvisited regions of the search space, while

Configuration	Population size	Target # generations
<b>S</b>	811	9230
<b>M</b>	1216	6340
<b>L</b>	1621	4700

Table 4: Population size and target number of generations for **S**, **M**, and **L** configurations.

crossover exploits information from existing solutions to accelerate convergence toward high-quality regions. The balance between these operators determines whether the algorithm emphasizes exploration or exploitation, thereby affecting convergence speed, solution diversity, and robustness to local optima. To study these effects, several combinations of  $p_m$  and  $p_c$  are evaluated for each population size. The resulting configurations are listed in Table 5.

Configuration	Population size	Mutation prob. $p_m$	Crossover prob. $p_c$
pm05-S	811	0.05	0.95
pm05-M	1216	0.05	0.95
pm05-L	1621	0.05	0.95
pm10-S	811	0.10	0.90
pm10-M	1216	0.10	0.90
pm10-L	1621	0.10	0.90
pm15-S	811	0.15	0.85
pm15-M	1216	0.15	0.85
pm15-L	1621	0.15	0.85
pm20-S	811	0.20	0.80
pm20-M	1216	0.20	0.80
pm20-L	1621	0.20	0.80

Table 5: Algorithm configurations used in the experiments. The identifier encodes the mutation probability  $p_m$  (pmXX =  $p_m = \text{XX}/100$ ) and the population sizes corresponding to configurations **S**, **M**, and **L**.

For each algorithmic configuration, populations obtained from different random seeds are combined prior to performance evaluation. To formalize this aggregation, we introduce the following sets:

- $E = \{1, 2, \dots\} \subseteq \mathbb{N}_0$ , the finite set of random seeds,
- $R = \{1, 2, \dots\} \subseteq \mathbb{N}_0$ , the finite set of generations,

We denote by  $P_{r,e}$  the population at generation  $r \in R$  for seed  $e \in E$ , where each element  $s \in P_{r,e}$  represents a single strategy. The final generation index is denoted by  $\tilde{r}$ . The combined population at generation  $r$  is then defined as

$$\bar{P}_r := \bigcup_{e \in E} P_{r,e}.$$

We define weak and strict dominance between two strategies  $s'$  and  $s$  over the four objectives  $LF_1(s)$ ,  $z(s)$ ,  $w(s)$ , and  $d(s)$  (see Section 3.2) respectively as

$$s' \preceq s \iff \forall f \in \{LF_1, z, w, d\} : f(s') \leq f(s),$$

and

$$s' \prec s \iff s' \preceq s \text{ and } \exists f \in \{LF_1, z, w, d\} : f(s') < f(s).$$

The *Pareto front* of a population  $P$  is the subset  $PF(P)$  is the set of strongly non-dominated strategies, defined as

$$PF(P) := \{s \in P \mid \nexists s' \in P : s' \prec s\}.$$

Although all weakly nondominated solutions are retained during the evolutionary process, Pareto front analysis is performed only on unique points. As a result, the reported fronts effectively consist of strongly nondominated strategies, ensuring that duplicate or equivalent solutions do not bias the evaluation.

The Pareto front at generation  $r$  is then given by  $PF(\bar{P}_r)$ , which represents the set of strategies that are non-dominated with respect to all strategies generated across different random seeds at that generation.

### 4.3 Evaluation Measures for MOEA

To evaluate the MOEA’s performance throughout the evolutionary process, two quantitative measures are employed. The first measure assesses convergence and diversity with respect to the optimal solution set, whereas the second measure evaluates how well the algorithm reproduces different dominance levels identified by the reference method, i.e., the block algorithm.

The first metric is the *Inverted Generational Distance Plus* ( $IGD^+$ ), which measures how closely the obtained solutions approximate the true Pareto front, i.e., the set of solutions generated by the block algorithm. Formally,  $IGD^+$  is computed by averaging, over all reference points on the true front, the minimum Euclidean distance to the set of solutions obtained by the MOEA, using a dominance-preserving distance measure [24]. Lower values of  $IGD^+$  indicate better convergence toward and coverage of the true Pareto front.

Before computing  $IGD^+$ , all objective values are normalized using min–max normalization. The normalization is performed with respect to the lower and upper bounds of each objective, defined by the ideal and nadir points of the objective space. For the discrete objectives, that is, topological depth, number of switches, and number of non-reference topologies, these bounds are known beforehand. For the continuous objective  $LF_1$ , the bounds are obtained from the best and worst feasible  $LF_1$  values produced by the block algorithm given the whole objective space (before nondominated sorting). The resulting normalization values are summarized in Table 6.

Objectives	Depth	Switches	Not ref. topo	$LF_1$
<b>Ideal</b>	0	0	0	77.3
<b>Nadir</b>	3	5	24	212.5

Table 6: Ideal and nadir objective values defining the bounds of the objective space.

The nadir values for depth and switches directly reflect the operational bounds imposed on the block algorithm:  $d^{\max} = 3$  corresponds to the maximum topological depth available in the dataset (see Table 2), and  $s^{\max} = 5$  is the maximum number of switching time steps allowed. These same bounds apply to the MOEA, ensuring that both methods operate over an identical search space.

Beyond the Pareto front itself, the block algorithm also identifies solutions belonging to subsequent dominance levels. The first level corresponds to the Pareto front, while the second level contains solutions dominated only by those in the first level, and so forth. Although solutions in higher dominance levels are suboptimal, they may still represent competitive trade-offs that are close to optimal with respect to specific objectives. Incorporating these additional fronts enables a more nuanced assessment of MOEA performance: even when the algorithm fails to recover all Pareto-optimal solutions, identifying solutions in lower dominance levels indicates partial convergence and meaningful progress toward optimality.

To quantify how well the MOEA reproduces these reference dominance fronts, we define the following performance measures:

$$I_k(P) := |PF(P) \cap F_k| \quad \text{and} \quad \hat{I}_k(P) := \frac{|PF(P) \cap F_k|}{|F_k|}, \quad (9)$$

where  $F_k$  denotes the  $k$ -th reference front obtained from the block algorithm, ordered by increasing dominance rank. The quantity  $I_k(P)$  counts the number of solutions in the MOEA Pareto front  $PF(P)$  that belong to the reference front  $F_k$ , while  $\hat{I}_k(P)$  normalizes this count by the size of  $F_k$ , yielding a relative coverage measure. Together, these metrics provide insight into both the absolute and relative ability of the MOEA to find solutions at different dominance levels. In this study, we consider  $k = 10$  different dominance levels.

Note that the cardinality of  $I_k(P)$  depends on how equality between solutions is defined across objectives. In particular,  $LF_1$  is the only continuous objective, whereas all other objectives are discrete. As a result, exact equality in  $LF_1$  values between MOEA solutions and reference solutions is unlikely, and without any numerical tolerance or rounding, the intersection  $PF(P) \cap F_k$  may be empty or contain only very few solutions, even when solutions are effectively equivalent in practice. To address this issue,  $LF_1$  values are first rounded. In our study, we round the  $LF_1$  values to the first decimal point.

Both  $IGD^+$  and the dominance-level coverage measures in Eq. (9) are computed per generation using the combined Pareto front  $PF(\bar{P}_r)$ . This allows the algorithm’s convergence behavior to be tracked over time, revealing not only the final solution quality but also the convergence rate and stability throughout the evolutionary process.

## 5 Results

In this section, we present the results obtained from the experiments described in Section 4. We begin by analyzing the solution set produced by the block algorithm, which serves as a reference for evaluating MOEA performance. Next, we compare the block algorithm with the MOEA by examining the distribution of dominance fronts in the final generation for each configuration listed in Table 5, using the performance indicators  $I_k(P)$  and  $\hat{I}_k(P)$  (see Section 4.3). We then analyze the MOEA’s convergence behavior over time using these indicators and the  $IGD^+$  metric. Finally, we provide a detailed inspection of the best-performing MOEA configuration.

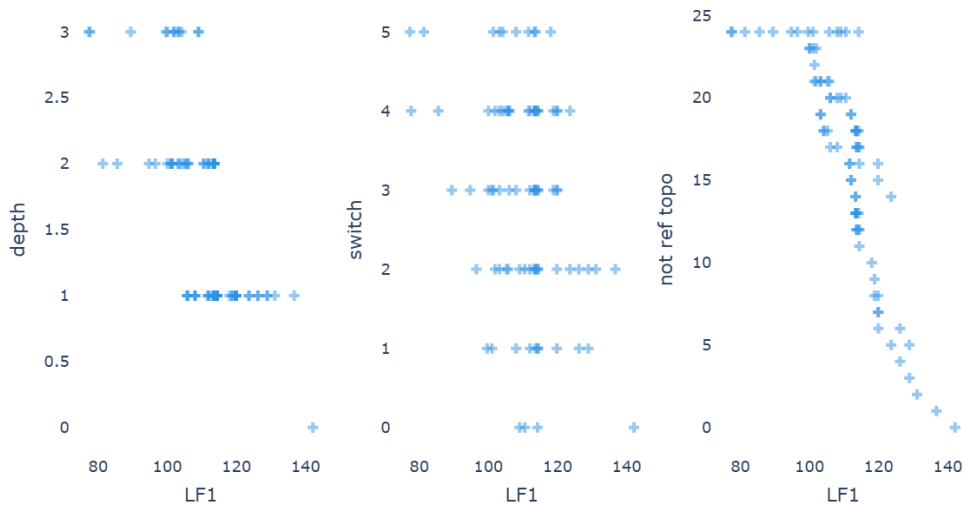


Figure 1: Distribution of Pareto-optimal solutions for the block algorithm. The solutions are plotted in terms of the objective  $LF_1$  and other objectives: topological depth (left), number of switching timestamps (center), and time steps not in the reference topology (right).

Figure 1 shows the objective values of the strategies identified by the block algorithm. Three key observations can be made:

- A strategy with a maximum  $LF_1$  value of approximately 80% can be achieved with a maximum topological depth of 3, requiring five switches and without relying on the reference topology.
- For the selected day, strategies achieving  $LF_1 < 100\%$  are only attainable when the reference topology is not used.
- In total, the block algorithm identifies 163,807,652 strategies, of which 83 correspond to unique points in objective space. This indicates that identical Pareto-optimal trade-offs can be realized by structurally distinct strategies.

Overall, the block algorithm provides system operators with a diverse set of high-quality strategies, enabling informed decision-making based on operational preferences and constraints. From an operational perspective, this shows that severe  $N - 1$  violations can be eliminated only by sustained, non-reference operation at higher topological depth.

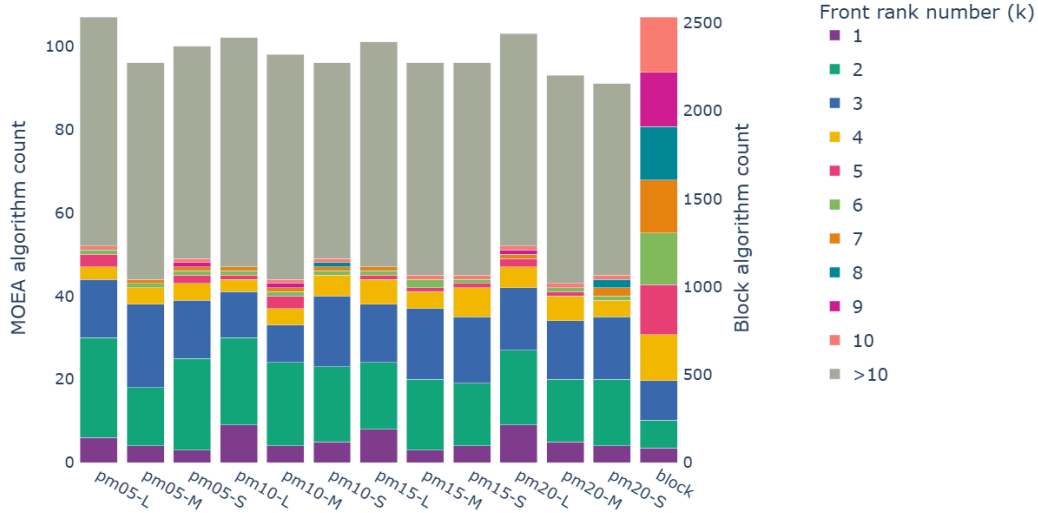


Figure 2: Frequency of distinct objective space points per dominance front rank ( $k$ ) in final combined populations. Lower rank fronts correspond to better trade-offs. For each MOEA configuration, the segments represent the count of recovered solutions per front, defined by  $I_k(P)$  (left y-axis, see Eq. (9)). For the block algorithm, the bar represents the total size of each reference front  $|F_k|$  (right y-axis).

Figure 2 shows the distribution of solutions across dominance fronts for the final combined Pareto front  $PF(\bar{P})$  obtained from each MOEA configuration, alongside the reference fronts produced by the block algorithm. Each bar on the x-axis corresponds to a specific MOEA configuration, while the rightmost bar represents the unique solutions identified by the block algorithm. The left y-axis reports  $I_k(\bar{P})$ , i.e., the number of MOEA solutions belonging to each reference front, while the right y-axis indicates the total number of points in each reference front. Gray bar segments correspond to solutions not recovered within the first ten dominance fronts.

The block algorithm identifies substantially more unique solutions than any MOEA configuration. Among the MOEA variants, larger population sizes consistently yield more solutions within the first 10 dominance fronts. In contrast, variations in mutation probability do not appear to significantly influence the distribution of recovered fronts.

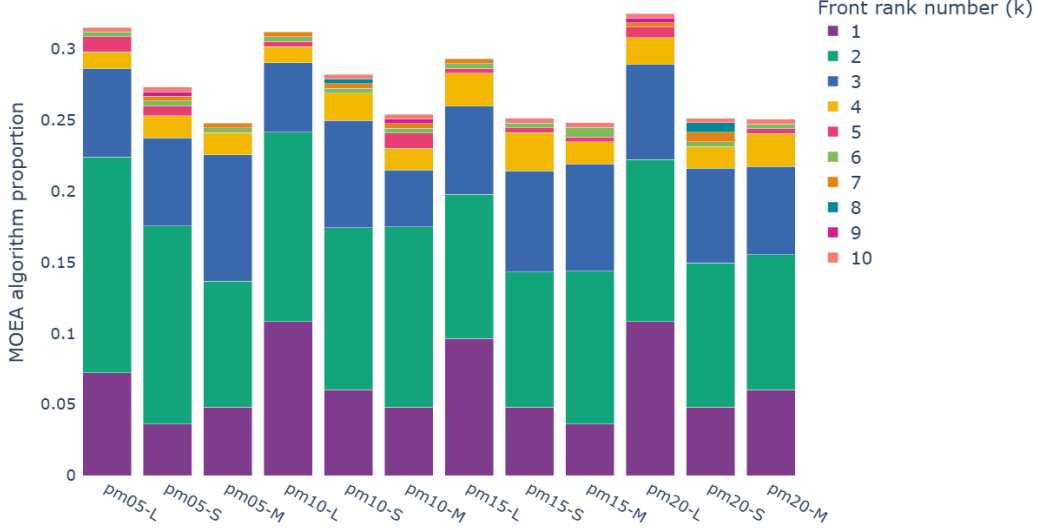


Figure 3: Relative coverage of reference dominance fronts ( $k$ ) across MOEA configurations. Lower rank fronts correspond to better trade-offs. The segments represent the proportion of unique solutions recovered from each reference front  $F_k$ , defined by the metric  $\hat{I}_k(P)$ , cf Eq. (9).

Figure 3 reports the relative coverage measure  $\hat{I}_k(P)$ , quantifying the proportion of solutions recovered by the MOEA relative to the total number of solutions in each reference front. Across all configurations, the MOEA recovers approximately 6% of the Pareto front and roughly 3–4% of all solutions within the first ten dominance fronts (note that it is not 30%–40% since we stack the results,  $10 \times 100\% = 1000\%$ ). This limited coverage is partly attributable to the restricted population sizes relative to the size of the reference fronts. Notably, the algorithm performs comparatively better on the second dominance front, recovering approximately 15% of its solutions.

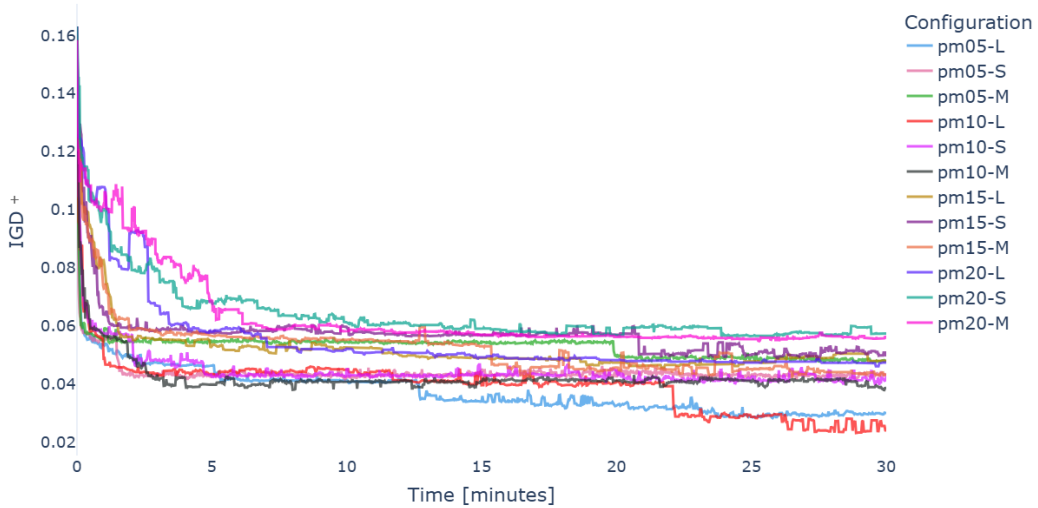


Figure 4: IGD<sup>+</sup> trajectories for all MOEA configurations over runtime. The x-axis denotes runtime in minutes, while the y-axis shows the normalized IGD<sup>+</sup> value.

Figure 4 presents the IGD<sup>+</sup> trajectories for all MOEA configurations. Across configurations, IGD<sup>+</sup> decreases rapidly during the first 5 minutes. After approximately 25 minutes, no further substantial improvements are observed. Configuration pm10-L achieves the lowest IGD<sup>+</sup> values, while pm20-S has the poorest convergence. Based on the IGD<sup>+</sup> metric, configuration pm10-L is selected for further

analysis.

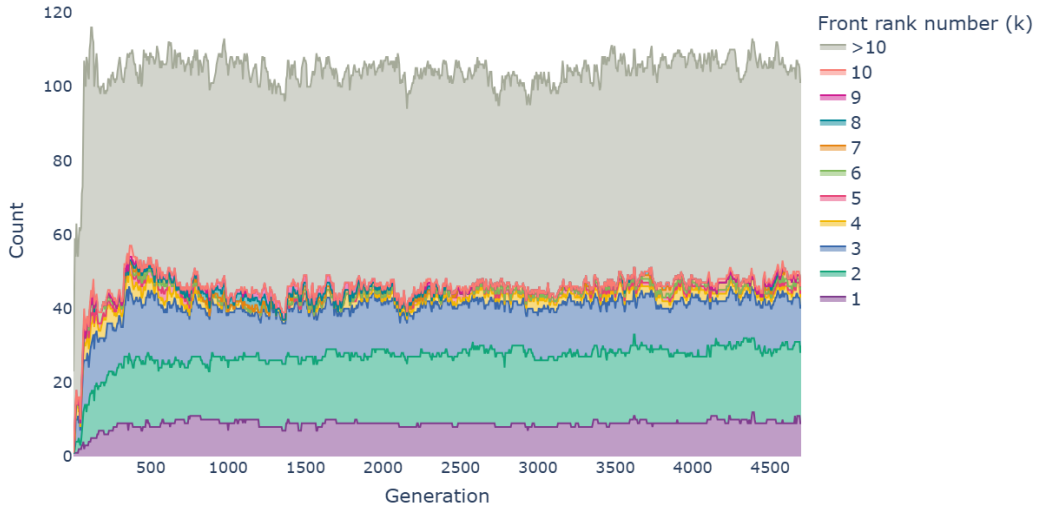


Figure 5: Evolution of dominance-front distribution for pm10-L over generations. Lower rank fronts correspond to better trade-offs. The x-axis represents the generation number, and the y-axis indicates the number of solutions. Each colored area corresponds to one of the first ten dominance fronts, while the grey area represents solutions outside the top ten.

Figure 5 illustrates the evolution of dominance-front membership across generations for pm10-L. Approximately 1,500 generations into the run, the distribution stabilizes, with roughly half of the population consistently belonging to the first ten dominance fronts.

Figure 4 shows that for pm10-L, the  $IGD^+$  drops around minute 23. This improvement is not reflected in Figure 5 because the number of Pareto points does not need to change; a superior point can be found that reduces the  $IGD^+$  value even if the total count of points in Front 1 remains constant.

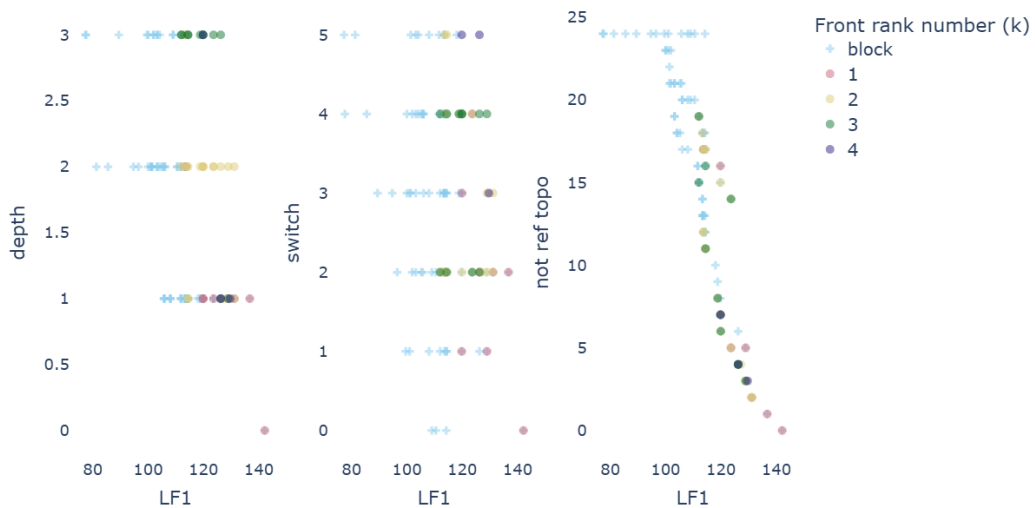


Figure 6: Objective-space distribution of final solutions for pm10-L. Lower rank fronts correspond to better trade-offs. Each subplot compares the LF1 values against one of the other objectives: topological depth (left), number of switches (center), and time steps not in the reference topology (right).

Figure 6 shows the final distribution of solutions across the first four dominance fronts for pm10-L.

PER FRONT					
Front $k$	MOEA (pm10-L)		Block algorithm		
	Points	Strategies	Points	Strategies	
1	9	23	83	$1.638 \times 10^8$	
2	21	54	158	$1.380 \times 10^{13}$	
3	13	30	225	$5.394 \times 10^{15}$	
4	5	7	261	$4.714 \times 10^{16}$	
5	2	2	283	$5.573 \times 10^{16}$	
6	1	1	294	$3.181 \times 10^{16}$	
7	2	2	301	$2.628 \times 10^{16}$	
8	1	1	305	$1.259 \times 10^{15}$	
9	1	1	309	$1.772 \times 10^{16}$	
10	1	1	314	$1.851 \times 10^{15}$	

CUMULATIVE					
Front $k$	MOEA (pm10-L)		Block algorithm		
	Points	Strategies	Points	Strategies	
1	9	23	83	$1.638 \times 10^8$	
2	30	77	241	$1.396 \times 10^{13}$	
3	43	107	466	$1.936 \times 10^{16}$	
4	48	114	727	$6.650 \times 10^{16}$	
5	50	116	1010	$1.222 \times 10^{17}$	
6	51	117	1304	$1.540 \times 10^{17}$	
7	53	119	1605	$1.803 \times 10^{17}$	
8	54	120	1910	$1.816 \times 10^{17}$	
9	55	121	2219	$1.993 \times 10^{17}$	
10	56	122	2533	$2.012 \times 10^{17}$	

Table 7: Distribution of results across dominance fronts for the best-performing MOEA configuration (pm10-L) and the block algorithm. For each front  $k$ , we report the number of distinct objective-space points and corresponding strategies, both per front and cumulatively.

While the block algorithm identifies solutions with  $LF_1 < 100\%$  for strategies with depth 2 or solutions involving a single switch, the MOEA does not find any solutions with  $LF_1 < 100\%$  across all fronts.

Table 7 shows how the points and strategies are distributed in the objective space. Most points and strategies are found on the first four fronts. On subsequent fronts, only a few additional points and strategies are found. The same table also shows how these results compare with the block algorithm and reveals a significant discrepancy between the number of strategies identified by the MOEA and those found by the block algorithm. Strategies are not enumerated individually by the block algorithm, but instead, for each nondominated configuration  $(d, M, \tilde{R})$ , the feasible strategy set is defined as the Cartesian product of the filtered topology sets associated with the blocks (see Eq. (4)). Every possible combination of available topologies across blocks constitutes a feasible strategy. As a result, a single objective point produced by the block algorithm can correspond to an enormous number of distinct strategies, on the order of millions or more.

In contrast, the MOEA explicitly represents each strategy as a chromosome in the population. Strategies exist only insofar as they are instantiated as individuals. Consequently, the total number of distinct strategies that the MOEA can ever hold at a given generation is upper-bounded by the population size. Moreover, each strategy must be explicitly generated using stochastic variation operators, such as crossover and mutation. This implies that newly generated strategies are typically close variants of existing ones.

This difference explains why the MOEA recovers only a small fraction of the strategies associated

with each objective point, even when many such strategies exist in principle. As shown in Figure 6, a substantial portion of the Pareto front produced by the block algorithm lies in the region where the number of non-reference topologies attains its maximum value. In this region, the MOEA identifies only a single solution in the fourth dominance front, indicating that this part of the search space is particularly difficult for the evolutionary approach to explore.

This behavior reflects the MOEA’s difficulty in reaching extreme regions of the search space. Configurations with many non-reference blocks lie at the boundaries of the Pareto front and are therefore structurally distant from the solutions typically encountered during the evolutionary process; as a result, they are underrepresented or missed entirely, even though the block algorithm readily identifies them.

In total, 14 Pareto-optimal points correspond to configurations in which all blocks are non-reference. Removing these from the 83 points on the first Pareto front leaves 69 points in regions that are more accessible to the MOEA. Within this reduced set of 69 accessible Pareto-optimal points, the MOEA recovers 13% (9 points) on its first front.

## 6 Discussion and conclusions

### 6.1 Summary of contributions

This paper formalized day-ahead transmission topology planning as a sequential multi-objective optimization problem with four operational objectives reflecting real TSO decision criteria: worst-case line loading under  $N - 1$  security, topological depth, number of switching actions, and time spent in non-reference topologies. Two solution methods were developed and compared using real operational data from the Dutch high-voltage grid operated by TenneT.

The proposed block algorithm exploits the temporal block structure of feasible strategies to enumerate the entire Pareto front exactly. With fixed operational bounds on maximum depth and switch count, its evaluation count grows only polynomially with the number of time steps, and it solves a highly congested day in under three minutes. Beyond providing optimal strategies, the block algorithm also serves as a benchmarking tool for other optimization approaches: its Pareto-front solutions define a reference set for distance-based metrics such as  $IGD^+$ , and its multi-front dominance structure enables a nuanced assessment that distinguishes full convergence from partial convergence.

A tailored MOEA was also developed, featuring direct variable-length encoding, structure-guided initialization across depth and switch counts, NSGA-III selection, and  $k$ -point crossover with random-reset mutation. The best-performing configuration (pm10-L) achieved the lowest  $IGD^+$  values and the broadest coverage of the top dominance fronts. Larger populations consistently improved front coverage, while mutation and crossover probabilities had a comparatively minor effect within the tested range. Nonetheless, no MOEA configuration recovered solutions with  $LF_1 < 100\%$ , whereas the block algorithm identified such solutions at low depth and with very few switches. Our findings suggest that, for the problem and objectives studied here, the block algorithm is the preferred method: it is exact and fast, with the ability to enumerate all feasible strategies and to identify every nondominated solution. However, MOEA approaches would nonetheless remain relevant in settings where the block algorithm cannot be directly applied, e.g., when additional objectives are added or more complex modeling assumptions are introduced.

### 6.2 Implications for grid operations

The results carry several practical implications for transmission system operators. First, the Pareto front reveals that strategies achieving  $LF_1 < 100\%$ , i.e., full  $N - 1$  security without any line overloading, require the reference topology to be abandoned entirely during the congested hours. This is a non-trivial operational insight: operators aiming for the highest security margins must accept topological configurations that differ from the default state throughout the day. Second, the block algorithm provides operators not with a single recommended action, but with a complete menu of Pareto-optimal strategies from which they can select according to their operational priorities on a given day. For example, favoring fewer switching actions during tight maintenance windows, or accepting strategies with a higher depth when  $N - 1$  security margins are the primary concern. Third, the fact that exact

enumeration is computationally tractable for a 24-hour horizon suggests that the block algorithm can be integrated into existing day-ahead congestion management workflows.

### 6.3 Limitations and future work

Several limitations of the present study should be acknowledged, each of which suggests directions for future research.

**Single-day evaluation** The analysis is based on a single highly congested operational day. While this provides a rigorous stress test, it does not capture the variability of congestion patterns across seasons, demand levels, and renewable generation profiles. Future work should apply the block algorithm to a representative sample of operational days to assess the robustness and generalizability of the findings.

**DC power flow approximation** All load-flow calculations use the DC approximation [38], which may diverge from full AC power flow results, potentially rendering some strategies suboptimal under more accurate models [26]. Furthermore, the power injections used as input are deterministic forecasts. Even state-of-the-art weather prediction models, which underpin generation and load forecasts, achieve approximately 90% accuracy for key variables such as precipitation and temperature [34]; the residual uncertainty can propagate into load-flow results and affect the quality of the recommended strategies. Incorporating stochastic or robust formulations that account for both DC-to-AC discrepancy and forecast uncertainty is an important avenue for future research.

**Preprocessing bottleneck** While the block algorithm identifies the Pareto front in under three minutes, it depends on a precomputed dataset of topology-level  $LF_1$  and depth values for every time step. Computing this dataset for the full set of available topologies across a 24-hour horizon is itself a substantial task. One promising direction to mitigate this bottleneck is the development of an imitation learning agent trained on block algorithm outputs [9, 10]: by learning to map grid conditions directly to high-quality switching strategies, such an agent could enable near-real-time decision support once trained offline.

**Objective completeness** The four objectives used in this study, while grounded in TenneT’s operational practice [39], do not capture all aspects of grid performance. Notably absent is a reliability metric such as the Loss-of-Load Probability (LOLP), which quantifies the risk that demand cannot be met [41]. Integrating such metrics would yield a more comprehensive assessment of strategy quality. More fundamentally, TenneT has identified a distance-based objective that minimizes the number of busbar operations required to transition between successive topologies. Because this objective depends on pairwise relations between topologies rather than on properties of individual topologies, it cannot be precomputed per block and therefore cannot be accommodated by the current block algorithm without structural redesign. The MOEA framework remains the natural vehicle for optimizing such objectives in the future.

**Mutation operator design** The random-reset mutation operator used in the MOEA directly affects the switching objective: each gene reset introduces an additional topology change, making offspring systematically inferior to their parents at high mutation rates. At a rate of  $p_m = 0.20$  applied to a chromosome of 24 genes, approximately 4.8 genes are reset on average, inflating the switching count by the same amount. Future work should investigate smaller mutation probabilities and, more broadly, self-adaptive mutation control [25], in which mutation parameters co-evolve with candidate solutions, eliminating the need for manual hyperparameter tuning.

**Scalability to larger grids** The current case study involves approximately 39,000 available topologies per time step. As the number of switchable substations grows (whether through grid expansion or finer-grained substation modeling), the collection of available topologies at every time step may increase by orders of magnitude, challenging the precomputation step on which the block algorithm depends.

Quantifying this scaling behavior and developing strategies to manage it (e.g., topology pre-screening heuristics) are important directions for extending the approach to larger networks.

## 6.4 Concluding remarks

Grid congestion is a growing and costly challenge for European transmission system operators, driven by the rapid integration of renewable generation and the slow pace of grid reinforcement [22, 1]. Topology reconfiguration offers a non-costly, immediately deployable congestion management measure that leverages existing infrastructure. This paper has shown that the combinatorial complexity of optimizing topological strategies over a full operational day, long perceived as intractable, can in fact be resolved exactly and efficiently by exploiting the problem’s temporal block structure. The block algorithm provides transmission operators with a complete set of Pareto-optimal strategies and a rigorous benchmark for evaluating any future heuristic or learning-based method developed for this problem class.

## Acknowledgements

The authors would like to thank TenneT TSO B.V. for providing access to the operational data used in this study. AI4REALNET has received funding from the European Union’s Horizon Europe Research and Innovation program under the Grant Agreement No 101119527. However, views and opinions expressed are those of the authors only and do not necessarily reflect those of the European Union. Neither the European Union nor the granting authority can be held responsible for them. The work of A. Zocca is partially supported by the NWO Vidi grant “*Power Network Optimization in the Age of Climate Extremes*” [GrantID 10.61686/GOOEL09973](#).

## Data availability

The operational data used in this study are derived from real-world grid data provided by TenneT TSO B.V. and are not publicly available. The dataset used in the analyses may be made available upon reasonable request, subject to the approval of TenneT TSO B.V.

## References

- [1] Agency for the Cooperation of Energy Regulators. Transmission capacities for cross-zonal trade of electricity and congestion management in the EU – 2025 market monitoring report. Technical report, ACER, 2025.
- [2] G. E. Andrews. *The Theory of Partitions*. Cambridge University Press, 1998.
- [3] H. Behnia and M. Akhbari. Integrated generation and transmission maintenance scheduling by considering transmission switching. *International Transactions on Electrical Energy Systems*, 29(4):e2792, 2019.
- [4] L. Beke, M. Weiszer, and J. Chen. A comparison of genetic representations and initialisation methods for the multi-objective shortest path problem on multigraphs. *SN Computer Science*, 2(3), 2021.
- [5] J. Chen, Q. Zhang, and G. Li. Moea/d for multiple multi-objective optimization. In H. Ishibuchi, Q. Zhang, R. Cheng, K. Li, H. Li, H. Wang, and A. Zhou, editors, *Evolutionary Multi-Criterion Optimization*, pages 152–163, Cham, 2021. Springer International Publishing.
- [6] Z. Chen. Optimal power flow in renewable-integrated power systems: A comprehensive review. *arXiv preprint arXiv:2408.05254*, 2024.
- [7] C. A. C. Coello, G. T. Pulido, and M. S. Lechuga. Handling multiple objectives with particle swarm optimization. *IEEE Transactions on Evolutionary Computation*, 8(3):256–279, 2004.

- [8] C. Coello Coello and M. Lechuga. Mopso: a proposal for multiple objective particle swarm optimization. In *Proceedings of the 2002 Congress on Evolutionary Computation. CEC'02 (Cat. No.02TH8600)*, page 1051–1056 vol.2. IEEE, 2002.
- [9] M. de Jong, J. Viebahn, and Y. Shapovalova. Imitation learning for intra-day power grid operation through topology actions. In M. Cerrato, editor, *Machine Learning and Principles and Practice of Knowledge Discovery in Databases*. Springer Nature Switzerland, 2024.
- [10] M. de Jong, J. Viebahn, and Y. Shapovalova. Graph neural networks for transmission grid topology control: Busbar information asymmetry and heterogeneous representations. *submitted*, 2026.
- [11] K. Deb and H. Jain. An evolutionary many-objective optimization algorithm using reference-point-based nondominated sorting approach, part i: Solving problems with box constraints. *IEEE Transactions on Evolutionary Computation*, 18(4), 2014.
- [12] M. Dorfer, A. R. Fuxjäger, K. Kozak, P. M. Blies, and M. Wasserer. Power grid congestion management via topology optimization with alphazero. November 2022.
- [13] A. E. Eiben and J. E. Smith. *Introduction to Evolutionary Computing*. Natural Computing Series. Springer, Cham, Switzerland, 2 edition, 2015.
- [14] E. B. Fisher, R. P. O’Neill, and M. C. Ferris. Optimal transmission switching. *IEEE Transactions on Power Systems*, 23(3):1346–1355, 2008.
- [15] G. Granelli, M. Montagna, F. Zanellini, P. Bresesti, R. Vailati, and M. Innorta. Optimal network reconfiguration for congestion management by deterministic and genetic algorithms. *Electric Power Systems Research*, 76(6-7):549–556, April 2006.
- [16] D. Hardin and E. Saff. Minimal riesz energy point configurations for rectifiable d-dimensional manifolds. *Advances in Mathematics*, 193(1):174–204, 2005.
- [17] K. W. Hedman, M. C. Ferris, R. P. O’Neill, E. B. Fisher, and S. S. Oren. Co-optimization of generation unit commitment and transmission switching with N-1 reliability. *IEEE Transactions on Power Systems*, 25(2):1052–1063, 2010.
- [18] K. W. Hedman, R. P. O’Neill, E. B. Fisher, and S. S. Oren. Optimal transmission switching with contingency analysis. *IEEE Transactions on Power Systems*, 24(3):1577–1586, 2009.
- [19] K. W. Hedman, S. S. Oren, and R. P. O’Neill. Optimal transmission switching: Economic efficiency and market implications. *Journal of Regulatory Economics*, 40:111–140, 2011.
- [20] K. W. Hedman, S. S. Oren, and R. P. O’Neill. A review of transmission switching and network topology optimization. In *Proc. IEEE Power and Energy Society General Meeting*, pages 1–7, 2011.
- [21] M. Heidarifar and H. Ghasemi. A network topology optimization model based on substation and node-breaker modeling. *IEEE Transactions on Power Systems*, 31(1):247–255, 2016.
- [22] International Energy Agency. Electricity grids and secure energy transitions. Technical report, IEA, Paris, 2023.
- [23] International Energy Agency. Grid congestion is posing challenges for energy security and transitions. IEA Commentary, 2025.
- [24] H. Ishibuchi, R. Imada, N. Masuyama, and Y. Nojima. Comparison of hypervolume, igd and igd+ from the viewpoint of optimal distributions of solutions. In *Lecture Notes in Computer Science (including subseries Lecture Notes in Artificial Intelligence and Lecture Notes in Bioinformatics)*, volume 11411 LNCS, pages 332–345. Springer Verlag, 2019.
- [25] O. Kramer. Evolutionary self-adaptation: A survey of operators and strategy parameters. *Evolutionary Intelligence*, 3:51–65, 08 2010.

- [26] H. W. Li, C. S. Wan, N. Ding, and W. J. Mao. Two successive approximate models and linear formulations for power flow analysis of dc grid. *Journal of Electrical Engineering and Technology*, 2024.
- [27] P. Li, X. Huang, J. Qi, H. Wei, and X. Bai. A connectivity constrained milp model for optimal transmission switching. *IEEE Transactions on Power Systems*, 36(5):4820–4823, September 2021.
- [28] H. Ma, Y. Zhang, S. Sun, T. Liu, and Y. Shan. A comprehensive survey on nsga-ii for multi-objective optimization and applications. *Artificial Intelligence Review*, 56(12):15217–15270, December 2023.
- [29] A. Marot, B. Donnot, C. Romero, B. Donon, M. Leroousseau, L. Veyrin-Forrer, and I. Guyon. Learning to run a power network challenge for training topology controllers. *Electric Power Systems Research*, 189, 2020.
- [30] M. Numan, M. F. Abbas, M. Yousif, S. S. M. Ghoneim, A. Mohammad, and A. Noorwali. The role of optimal transmission switching in enhancing grid flexibility: A review, 2023.
- [31] M. Numan, D. Feng, F. Abbas, S. Habib, and A. Rasool. Mobilizing grid flexibility through optimal transmission switching for power systems with large-scale renewable integration. *International Transactions on Electrical Energy Systems*, 30(3):1–15, March 2020.
- [32] R. P. O’Neill, K. W. Hedman, E. A. Krall, A. Papavasiliou, and S. S. Oren. Economic analysis of the n-1 reliable unit commitment and transmission switching problem using duality concepts. *Energy Systems*, 1(2):165–195, January 2010.
- [33] F. Pranjčić and P. Vrtič. Analysis of the operational reliability of different types of switching substations using the monte carlo method. *Energies*, 17, 7 2024.
- [34] M. S. Rahman, F. A. Tumpa, M. S. Islam, A. Al Arabi, M. S. B. Hossain, and M. S. Ul Haque. Comparative evaluation of weather forecasting using machine learning models. In *26th International Conference on Computer and Information Technology (ICCIT)*, page 1–6. IEEE, Dec. 2023.
- [35] R. P. Stanley. *Enumerative Combinatorics, Volume 1*. Cambridge University Press, 2011.
- [36] G. Thomassen, A. Fuhrmanek, R. Cadenovic, D. Pozo Camara, and S. Vitiello. Redispatch and congestion management. Jrc137685, European Commission, Joint Research Centre, 2024.
- [37] E. van der Sar, A. Zocca, and S. Bhulai. Optimizing power grid topologies with reinforcement learning: A survey of methods and challenges. *Foundations and Trends in Electric Energy Systems*, 9(1):1–119, July 2025.
- [38] J. van Dijk, J. Viebahn, B. Cijssouw, and J. van Casteren. Bus split distribution factors. *IEEE Transactions on Power Systems*, 39(3):5115–5125, 2024.
- [39] J. Viebahn, S. Kop, J. Van Dijk, H. Budaya, M. Streefland, D. Barbieri, P. Champion, M. Jothy, V. Renault, and S. Tindemans. Gridoptions tool: Real-world day-ahead congestion management using topological remedial actions. *CIGRE Science & Engineering*, 35:1–15, 2024.
- [40] J. Viebahn, M. Naglic, A. Marot, B. Donnot, and S. H. Tindemans. Potential and challenges of AI-powered decision support for short-term system operations. In *CIGRE Paris Session 2022*. CIGRE, 2022.
- [41] C. Zhang and J. Wang. Optimal transmission switching considering probabilistic reliability. *IEEE Transactions on Power Systems*, 29(2):974–975, March 2014.
- [42] Y. Zhou, A. S. Zamzam, A. Bernstein, and H. Zhu. Substation-level grid topology optimization using bus splitting. In *2021 American Control Conference (ACC)*, page 1–7. IEEE, May 2021.
- [43] E. Zitzler and S. Künzli. Indicator-based selection in multiobjective search. In X. Yao, E. K. Burke, J. A. Lozano, J. Smith, J. J. Merelo-Guervós, J. A. Bullinaria, J. E. Rowe, P. Tiño, A. Kabán, and H.-P. Schwefel, editors, *Parallel Problem Solving from Nature - PPSN VIII*, pages 832–842, Berlin, Heidelberg, 2004. Springer Berlin Heidelberg.